

A Twisted Four-Sheeted Model for an Amyloid Fibril

Jimin Wang,^{1,*} Susanne Gülich,¹
Catharine Bradford,¹ Marina Ramirez-Alvarado,³
and Lynne Regan^{2,*}

¹Department of Molecular Biophysics
and Biochemistry

²Department of Chemistry
Yale University
266 Whitney Avenue
New Haven, Connecticut 06520

Summary

The formation of amyloid fibers and their deposition in the body is a characteristic of a number of devastating human diseases. Here, we propose a structural model, based on X-ray diffraction data, for the basic structure of an amyloid fibril formed by using the variants of the B1 domain of IgG binding protein G of *Streptococcus*. The model for the fibril incorporates four β sheets in a bundle with a diameter of 45 Å. Its cross-section, or layer, consists of four strands, one strand from each sheet. Layers stack on top of each other to form the fibril, which has an overall helical twist with a periodicity of about 154 Å. Each strand interacts in a parallel fashion with the strands in the layers above and below it, in an infinite β sheet. Some geometric features of this model and the logic behind it may be applicable for constructing other related cross- β amyloid fibrils.

Introduction

Amyloid fiber formation and deposition are associated with many human diseases, Alzheimer's, type II diabetes, and Creutzfeldt-Jakob being well-known examples. The proteins that form fibers in disease-associated states or that can be induced to form fibers in vitro have very different sequences and three-dimensional structures. Nevertheless, the fibers that are formed share many common features. Each fiber is composed of a single type of protein; the fibers are straight, unbranched, and of a similar width; and they bind certain dyes such as Thioflavin T and Congo red with a characteristic enhancement of fluorescence and birefringence (Puchtler et al., 1961; Naiki et al., 1989; Serpell, 2000; Dobson, 2003).

Fiber diffraction studies on a number of different amyloid fibers, from both ex vivo and in vitro sources, reveal additional common features: strong reflections at about 4.7–4.8 Å and 10–11 Å that have been interpreted in terms of a cross- β structure (Sunde et al., 1997; Serpell, 2000). Various models for fibers have been pro-

posed on the basis of fiber diffraction, solid-state NMR, and electron microscopy studies (Jimenez et al., 1999, 2002; Serpell, 2000; Serpell and Smith, 2000; Petkova et al., 2002; Diaz-Avalos et al., 2003; Sikorski et al., 2003). The identity of actual toxic species is not known; for example, there are suggestions that small, soluble oligomers may be of importance for amyloid diseases (Bucciantini et al., 2002). Nevertheless, a more detailed model for the amyloid fiber is essential for a more complete understanding of the nature of this state and for any rational attempt to either prevent or reverse fiber formation.

Several groups have reported the advantages of studying fiber formation in vitro with proteins that are not necessarily associated with disease in vivo (Jimenez et al., 1999; Gujjarro et al., 1998; Chiti et al., 1999; Gross et al., 1999; Ramirez-Alvarado et al., 2000, 2003; Bucciantini et al., 2002; Ramirez-Alvarado and Regan, 2002). These studies allow the common thermodynamic and kinetic features of fiber formation to be elucidated in systems that can be more readily characterized.

We have used variants of the B1 domain of IgG binding protein G from *Streptococcus* (Björck and Kronvall, 1984; Åkerström et al., 1985) as an accessible model system to study amyloid fiber formation (Ramirez-Alvarado et al., 2000, 2003; Ramirez-Alvarado and Regan, 2002). The structure of the native fold of the B1 domain is known at high resolution (Figure 1A) (Gronenborn et al., 1991; Gallagher et al., 1994; Kuszewski et al., 1999), and the kinetics of folding and the thermodynamics of stabilization have been studied extensively (Alexander et al., 1992a, 1992b; Smith et al., 1994; Smith and Regan, 1995; Merkel and Regan, 1998; Merkel et al., 1999). The protein can be purified from *Escherichia coli* in large quantities, and virtually any sequence variant desired can be readily created. We have defined conditions in which mutants of the B1 domain reproducibly and predictably form fibers (Figure 1) (Ramirez-Alvarado et al., 2000, 2003; Ramirez-Alvarado and Regan, 2002). Fiber formation shows typical lag-phase kinetics, which can be overcome by seeding with small amounts of preformed fibers. The B1 fibers show all of the structural and physical properties of typical disease-associated fibers.

Here, we present the results of X-ray diffraction studies on a partially aligned variant of B1 fibers, and of fibers in a polycrystalline state, which allow us to construct a structural model for the cross- β structure of an amyloid fibril. Some of the geometric relationships within this model and the logic for deriving it may be applicable for constructing other related cross- β amyloid fibrils.

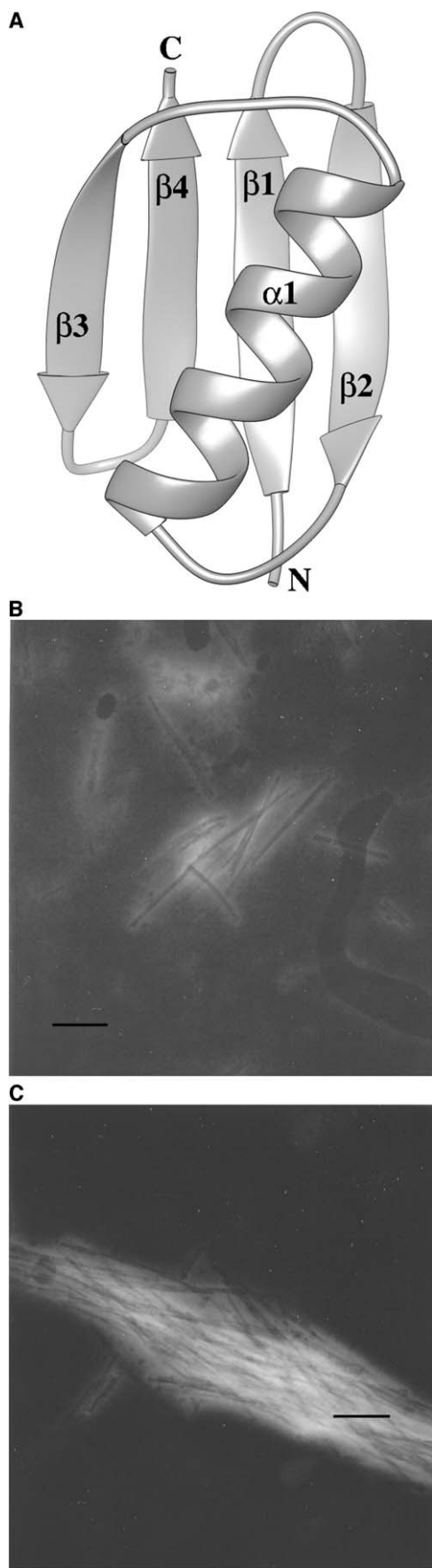
Results and Discussion

Formation and X-Ray Diffraction of B1 Amyloid Fibrils

The formation of B1 fibrils was monitored with electron microscopic imaging by following an established pro-

*Correspondence: jimin.wang@yale.edu (J.W.); lynne.regan@yale.edu (L.R.)

³Present address: Department of Biochemistry and Molecular Biology, Mayo Clinic and Foundation, 200 First Street, SW, Rochester, Minnesota 55905.



cedure (Ramirez-Alvarado et al., 2000, 2003; Ramirez-Alvarado and Regan, 2002). The fibril formation was highly reproducible from one preparation to another, with some variations in the length of formed fibrils and the degree of their clustering (Figures 1B and 1C). The samples contained no natively folded B1 monomers, which were depleted upon fibril formation, and any residual unpolymerized protein was removed by repetitive centrifugation and extensive washing of the fibers. Other than NaCl, the samples contained no additional chemicals that might interfere with X-ray diffraction experiments when dried. The prepared fibers were resuspended in 0, 50, and 100 mM NaCl/distilled water, a range of NaCl concentrations previously known to induce the fiber alignment (Oda et al., 1998; Yamashita et al., 1998).

Partially dried samples of preformed fibrils of a number of B1 variants, including the B1(A_Y) variant (Merkel and Regan, 1998; Ramirez-Alvarado et al., 2000, 2003; Ramirez-Alvarado and Regan, 2002), were prepared. X-ray diffraction analysis showed one strong reflection at 4.8 Å and one weak reflection at 10.1 Å in all variants (Figure 2). The resolution of observed reflections was determined upon calibration by using the powder diffraction of NaCl as a reference. The intensity of the observed reflections, relative to background scattering by solvent, increased substantially as the packing density of the fibrils increased upon drying.

Fiber alignment was carried out in order to assign the two observed reflections to geometric locations with respect to the fiber axis, and thus to determine the underlying structural elements. We used horizontal centrifugation at 2000 × g at 4°C for extended periods (days to weeks) and a stretching frame to align the preformed B1(A_Y) fibers. The sufficient alignment allowed us to make an assignment of the 4.8 Å spacing to the meridional direction, i.e., parallel to the fiber axis, and the 10.1 Å spacing to the equatorial direction, i.e., perpendicular to the fiber axis (Figures 2C–2E). Our observation is consistent with results from fiber diffraction studies reported for several other amyloid fibers (Sunde et al., 1997; Serpell et al., 2000; Balbirnie et al., 2001; Diaz-Avalos et al., 2003; Sikorski et al., 2003). A common feature of all of these amyloid fibers is a cross-β structure in which the sheet normal (a vector perpendicular to the sheet) and the strand direction are perpendicular to the fiber axis. In this model, the 4.8 Å reflection corresponds to the strand-strand spacing, and the 10.1 Å reflection corresponds to the sheet-sheet spacing (Sunde et al., 1997; Serpell, 2000). The existence of the 10.1 Å reflection suggests that there are two or more sheets in fibrils, excluding the possibility of single-sheeted amyloid models such as those

Figure 1. The A_Y Mutant of the IgG Binding B1 Domain of Streptococcal Protein G

(A) A ribbon diagram of the B1 domain (Gronenborn et al., 1991). The α helix diagonally crosses the four-stranded β sheet.

(B and C) TEM images of the A_Y mutant fibers. Fibers were applied to formvar-coated copper grids and negatively stained with 1% PTA. Scale bars, 1000 Å.

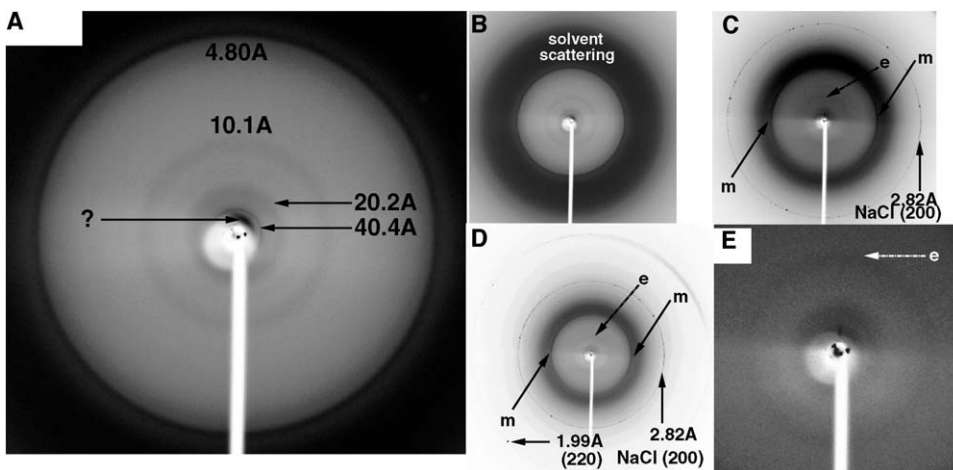


Figure 2. X-Ray Fiber Diffraction of the AY Mutant Fibrils

(A) The fibrils were resuspended in water and air dried. There are at least four defined reflections whose resolution is indicated. The resolution of the potential fifth reflection could not be independently determined. (B) A zoom-out of (A). (C–E) Partial fiber alignment. (C) Partial alignment along the capillary direction resulted in indexing of meridional (m) and equatorial (e) reflections. The NaCl (200) reflection is also indicated. (D) A second sample with meridional and equatorial reflections indicated. Two NaCl reflections, (200) and (220), are also shown. (E) An enlargement of (D) shows an equatorial reflection. The exposure time for (A) was 3 hr, and the exposure time for (C) and (D) was 90 min.

in a β helix structure (Govaerts et al., 2004) or in a natively folded single-sheeted protein (Koide et al., 2000).

Two additional reflections, one at 20.2 Å and the other at 40.4 Å, were observed in many of the B1(AY) fiber samples (Figure 2A). Because of weak intensity, these two reflections could not be directly assigned. They are indirectly assigned to equatorial reflections because of a simple arithmetic relationship to the 10.1 Å equatorial reflection. The observation of the 20.2 Å reflection suggests that there exist at least three sheets in amyloid fibrils. Although the 40.4 Å reflection is also an equatorial reflection, it does not correspond to five sheets in the amyloid fibrils. This is a very sharp Bragg reflection, corresponding to lattice spacing in the polycrystalline state (see below).

Formation and X-Ray Diffraction of Polycrystalline B1(AY) Amyloid Fibrils

Packing and alignment of preformed fibers is analogous to the crystallization process of globular proteins, except that preformed fibers are not freely diffusible and do not undergo large thermal motions in solution. Unlike globular proteins, preformed fibers are sensitive to macroscopic forces such as mechanical force (centrifugation and stretching techniques) and electromagnetic force, which are known to promote the alignment of proteinaceous fibers (Guijarro et al., 1998; Malinchik et al., 1998; Oda et al., 1998; Yamashita et al., 1998; Sikorski et al., 2003). Controlled dehydration, i.e., drying the samples, is another important factor in fiber alignment. Dehydration of the B1(AY) fibers greatly improved the diffraction quality of our samples (Figures 2B and 2D).

Six samples of preformed B1(AY) fibrils in capillary tubes were set for alignment. The alignment was monitored by X-ray diffraction, which was performed after each extended period (in days and weeks) of centrifuga-

tion at 4°C and dehydration at room temperature. This procedure was repeated 4–8 times in a period of 6 months. No changes in diffraction patterns were observed when dehydration was complete after 3–5 months. Similar results were obtained when a stretching frame method was used. Of six samples, one had gradually improved the diffraction quality to at least 1.6 Å resolution, but without any signs of global alignment.

We have observed reflections from 154 to 1.6 Å resolution from one B1(AY) amyloid fiber sample in the crystalline state or in the powder form of amyloid fiber crystals (Figure 3). In order to exclude all reflections from NaCl and other obscure reflections derived from the detector/beam stop geometric setup, calibration images derived from using the powder of NaCl were taken immediately after (Figure 3B) and before (data not shown) an experimental image (Figure 3A). Each NaCl single crystal has three reflections, (200) at 2.821 Å, (220) 1.994 Å, and (222) 1.628 Å, observable in the resolution range. Many NaCl single crystals were sparsely present in various locations of the sample. In order to make sure that amyloid fibers were a homogenous species, X-ray diffraction was carried out in five different locations of the sample within the capillary. An image from a location with the fewest NaCl reflections was used for detailed analysis (Figure 3A). This image still has three NaCl reflections behind the inset of Figure 3A, which affected the accuracy of resolution determination for reflections nearby even after they were masked out for analysis. All reflections from amyloid fibers have the same half-peak width as the calibration NaCl powder sample, and this finding is expected based on the fact that the X-ray beam size determines the half-peak width.

This sample also had typical broad reflections at 4.8 Å and 10.1 Å resolutions at the early stage of alignment. These two reflections were absent in the final polycrys-

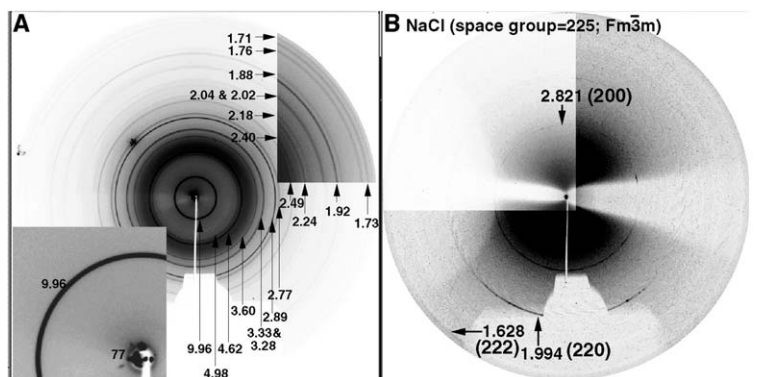


Figure 3. X-Ray Powder Diffraction of the Polycrystalline State of the AY Fibril

(A) Fibrils were resuspended in 50 mM NaCl and air dried. Resolutions of the reflections were calibrated by using the NaCl (200) reflection. Note that reflections at 76.8 Å (77 Å) and a lower resolution (estimated to be 153.6 Å) are from the polycrystalline state of the fibrils. Three individual reflections at 2.821 Å, 1.994 Å (behind the inset), and 1.628 Å are (200), (220), and (222) reflections, respectively, from one single NaCl crystal present in the fiber sample.

(B) Powder diffraction of NaCl in a calibration experiment.

talline state, implying that a transition from an un-packed to a well-packed lattice-defined polycrystalline state of amyloid fibers was completed.

Indexing and Unit Cell Dimensions of Polycrystalline B1(AY) Fibrils

Indexing of the fibril diffraction pattern was carried out in a two-dimensional lattice and resulted in a square lattice with $a = b = 39.83$ Å for all reflections (Figure 4), with the exception of the two lowest-resolution reflections. With this lattice, the maximal discrepancy in resolutions between the observed and predicted reflections was 0.017 Å, and the mean discrepancy was 0.011 Å for all 17 strong reflections (Figure 4) plus an additional 12 weak reflections (not shown). Reflections with large resolution discrepancies were near NaCl reflections.

The two observed lowest-resolution reflections, one at 76.8 Å resolution and the other at about 153.6 Å, were assigned to be the third orthogonal cell edge dimension. The precise resolution of the lowest-resolution reflection was determined with an error of about

5 Å due to the fact that it was too close to the beam stop and was back calculated from 32×4.8 Å (see below). With this indexing, the primitive unit cell dimensions are $a = b = 39.83$ Å, $c = 153.6$ Å, $\alpha = \beta = \gamma = 90^\circ$. This unit cell should contain one crystallographic unit of fibrils.

Two geometric factors of the fibers in the polycrystalline state may explain why only a small fraction of reflections are observable for the large unit cell. Here, unlike with powder diffraction of NaCl crystals, we have a severe overlapping problem among reflections. For a reflection in a given resolution, its intensity is distributed in the detector area that is proportional to the square of the resolution, and the number of the nearby reflections that contribute to background is proportional to the cube of the resolution. This feature makes the disproportionately large number of reflections unobservable. In fact, with the assistance of one of us (J.W.), Martin and Zilm (2003) have observed that the number of observable reflections from thousands and ten of thousands in single crystals of five proteins was rapidly reduced to only a dozen after they were converted to microcrystals and finally to nanocrystals.

However, the geometric basis for missing strong reflections at low resolutions is different. Between 9.96 Å and 76.8 Å, there was a very weak reflection at about 40 Å, observed only after integration. This reflection corresponds to the first order of the reflection of the square lattice. Two reasons may explain why it is so. First, the long unit cell dimension may be highly disordered with the diffraction limit of about 77 Å resolution. Second, which is a more likely possibility, a very large rising angle in the helical structure may have resulted in a large blind diffraction cone (Cochran et al., 1952; Wilkins et al., 1953; Taylor and Lipson, 1965). This cone along the fiber axis (or the l direction) started with $l = 0$ and had an angle of 60° . This included virtually all non-zero l index reflections with small indexes of h and k (see Experimental Procedures for computational verification and estimation of the core angle).

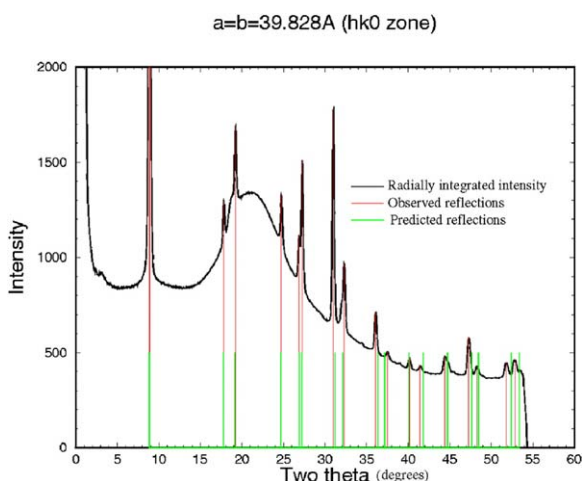


Figure 4. Indexing of Radially Integrated Reflections

Only the ($hk0$) zone is indexed. The vertical axis is measured in relative intensity, and the horizontal axis is measured in degrees. Less well-matched reflections at high two theta angles are likely due to the contribution of zones with $l = 1$ or higher values.

Unit Cell Content and the Concept of the Basic Amyloid Fiber-Forming Unit

The first-order reflection along the long axis has been determined to 153.6 Å upon retrospective calculation from 32×4.8 Å. It is important to note, however, that

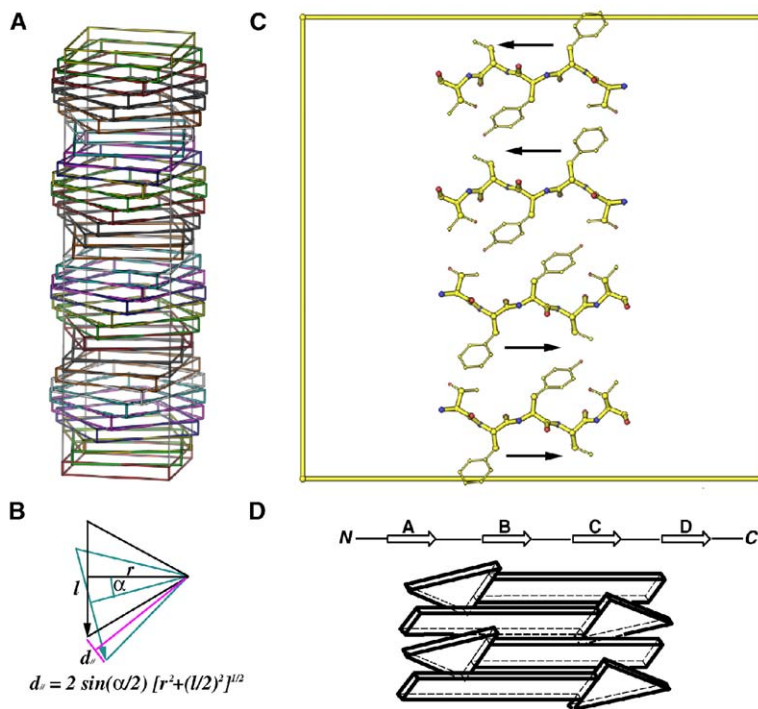


Figure 5. The Slab Concept of a Basic Amyloid Fiber-Forming Unit

(A) The unit cell can be sliced into 32 equal slabs, and the slabs are continuously twisted around the fiber axis. The twisting of slabs neither changes the volume of the unit cell nor affects the packing of unit cells in the lattice.

(B) The twisting of slabs causes a corner-to-corner displacement of two adjacent slabs. Thus, the projected end-to-end displacement ($d_{//}$) of their strands onto the slab, as formulated, is a function of the distance (r) to the twisting axis, the twisting angle (α), and the length (l) of the strands. One way to prevent the end-to-end distance from increasing is through their strand-to-strand backbone hydrogen bonds after the strands are properly tilted (see text).

(C and D). Two possible arrangements of four β strands within each slab and their relationship with the protein sequence: a (C) mixed parallel/antiparallel mode and an (D) all-alternating antiparallel mode with a pseudo dyad at the center. (C) The crystallographic data of $a = b = 39.83 \text{ \AA}$ suggest four independent β sheets within each slab. Each subunit contributes four segments, labeled as A, B, C, and D on the protein sequence in (D), for the formation of four β strands in the amyloid fibers, which may not be the same

as $\beta 1$, $\beta 2$, $\beta 3$, and $\beta 4$ in their native structure (Figure 1A). The one-to-one relationship between the four strands on the protein sequence and the four strands within each slab remains unknown. Atomic structures of four strands (all having the same TFYVT sequence) in (C) is *only* for demonstration of the strand-strand distance within each slab (which is actually the sheet-sheet distance within the fibers), the pattern of the backbone hydrogen bonds (which are formed between slabs and vertical to the plane), and the location of their side chains (which is within each slab and horizontal to the plane).

the conclusions drawn in this study are independent of whether it is actually 31, 33, or 32 times 4.8 \AA .

The unit cell can accommodate 32, 16, or 8 B1 domain monomers with corresponding solvent contents of 0.0%, 50.0%, and 75.0%, assuming that the protein density in these amyloid fibers is the same as (or higher than) that typically observed in crystals of native proteins. Because the high-resolution powder diffraction data were obtained from a dried fiber sample, it is extremely unlikely that there was a large solvent content in the unit cell. Therefore, a model of 32 monomers in 1 unit cell, with a 0% solvent content, is by far the most reasonable choice.

When the entire unit cell is sliced into 32 equal slabs along the long unit cell edge, each monomer occupies one slab within its side dimension of $40 \times 40 \text{ \AA}$ and a height of 4.8 \AA (Figure 5A). The slab is the basic amyloid fiber-forming unit and a minimal noncrystallographic unit, from which the entire unit cell content can be generated by using 32-fold helical noncrystallographic symmetry (NCS).

Number of β Sheets in the Amyloid Fiber Model

When the slab is added onto a growing chain of amyloid fibers one at a time, backbone hydrogen bonds are formed between the newly added slab and the existing fiber while hydrophobic residues are buried within the fiber (Figure 5). Therefore, the number of strands in the slab is equivalent to the number of sheets in the amyloid fiber.

Our X-ray data described above show that there exist at least three sheets. The three-sheeted fiber, i.e., the three-stranded slab of about 30 \AA in width, would require us to propose 10 \AA of some type of ordered structure at its sides in order to generate the well-defined lattice dimension of 40 \AA . Conversely, there is not sufficient space in the unit cell for a five-stranded layer. Therefore, our data support that there are four sheets in the fiber and four strands in each slab.

Arrangement of Parallel β Strands within Each Sheet

Each strand in each slab forms one continuous sheet, in which the backbone hydrogen bonds are formed between layers that are stacked along the long axis of the fiber. The orientation of equivalent strands between two adjacent slabs is largely identical (with a slight twisting as described below), i.e., β sheets are made of all-parallel β strands. Consistent with our parallel in-register architecture of the β sheet model, other similar models have been proposed, including ones for $A\beta_{1-40}$ determined by solid-state NMR and α -synuclein with EPR labeling (Petkova et al., 2002; Der-Sarkissian et al., 2003).

The X-ray data we present favor one monomer per slab (monomeric slab), over both two (dimeric) and four (tetrameric) monomers per slab. The three models of slabs differ in volume and height (4.8 , 9.6 , and 19.2 \AA , for monomeric, dimeric, and tetrameric models, respectively), the number of helical symmetry (32-, 16-,

and 8-fold, respectively), and the successive rotation ($360^\circ/32$, $360^\circ/16$, and $360^\circ/8$, respectively) between two adjacent slabs. The observation of the single 4.8 Å equatorial reflection in the X-ray diffraction data suggests that only the monomeric slab model is possible. The absence of 9.6 Å and 19.2 Å reflections, corresponding to the primitive repeats for the dimeric and tetrameric slab models, excludes both of them. The monomeric slab model is the most consistent with the observed large blind cone in the diffraction data (see [Experimental Procedures](#)) and requires the least amount of reorientation of strands between two successive slabs for maintaining backbone hydrogen bonds ([Figure 5A](#)). Because only in the dimeric and tetrameric models is an antiparallel arrangement of β strands in sheets possible, the X-ray diffraction data we present have then excluded such an arrangement in our amyloid fibers. Nevertheless, in the literature, antiparallel arrangement models have been proposed for other amyloid fibers ([Gordon et al., 2004](#); [Petkova et al., 2004](#); [Makin et al., 2005](#)).

In the twisted fibers, as described below, one can picture each sheet as wrapping tangentially around a cylindrical surface ([Figure 6](#)). The curvatures of two outer sheets, with a distance of about 20 Å to the central fiber axis, and the two inner sheets, with a distance of about 10 Å, are different.

The sheet curvature of all-parallel strands depends on a given amino acid sequence of strands. Consider, for example, a β sheet made of 5-residue β strands, of sequence AANAA. The interstrand distance of about 4.7–4.8 Å for the backbone H bonds is also ideal for the asparagine-asparagine side chain-side chain H bonds, and little twisting of the sheet is observed. Compare this situation with a β sheet that is still made of 5-residue β strands but has strands of sequence AAFAA. For this sequence, much more significant twisting of the β sheet is required to accommodate the phenylalanine-phenylalanine side chain-side chain stacking interaction, which is about 3.7–3.9 Å. The extent of β sheet twisting is clearly a function of accumulative interactions of all 5 residues on the strands. Therefore, any β sheet of all-parallel strands made of any given peptides has its own preferred twisting and curvature.

Arrangements between β Sheets

The four β sheets in our slab have a defined polarity; one edge corresponds to the C termini, and the other corresponds to the N termini. The arrangement of four sheets is defined by the arrangement of four strands within each monomeric slab. Two possible arrangements of the four strands are shown in [Figures 5C](#) and [5D](#): a mixed parallel/antiparallel mode and an all-alternating antiparallel mode. These are the only two possible modes. In these modes, connections between strands are made of very short loops that are located on the same side of sheet edges. The all-parallel arrangement of four strands within our slab requires much longer loops and is not possible, because in the current model, only about half of the residues of each monomer are available for making the connection loops. However, the precise sequence from this protein contributing four strands and the one-to-one relationship between the

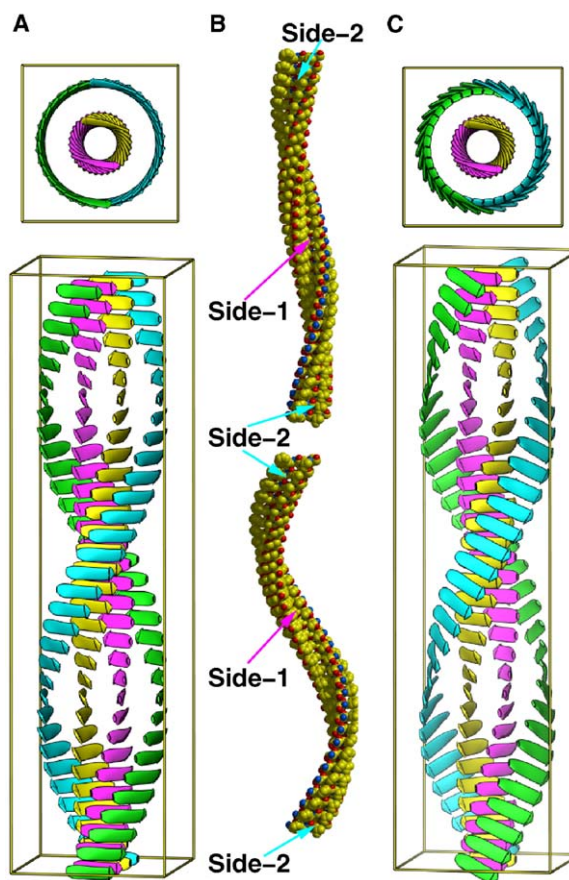


Figure 6. Two Twisted Four-Sheeted Models with and without Tilting of Strands

(A) Two orthogonal views of one unit cell.

(B) Surface properties of the β sheets. An inner β sheet (upper model) requires side chain interactions within the sheet and with other sheets at both sides with a small curvature. An outer β sheet (lower model) requires side chain interactions at only one side (side-1) with a large curvature. Side-2 is exposed to the solvent.

(C). A similar model as (A), but the β strands in the outer sheets tilt about 35° in order to maximize all backbone hydrogen bond interactions within the β sheets.

four strands in the sequence and the four strands in one slab ([Figure 5](#)) are beyond the scope of this study and will be addressed elsewhere.

Four strands in each monomeric slab belong to one single polypeptide and are subject to a connectivity constraint ([Figure 5](#)). In the natively folded β sheets of all-parallel strands, connecting loops may run cross-over at the sides of β sheets. In the amyloid fibers, one β sheet stacks against another, and the sheet extends infinitely, forming impassable walls. Crossover topology is no longer permissive when the number of amino acids in connecting loops is limited. This connectivity constraint does not exist for small peptides used for studying amyloid fiber formation.

Helical Twisting of Amyloid Fibers and β Sheets

A key observation in our X-ray diffraction data is a long repeat edge of 153.6 Å, corresponding to 32 slabs of

fibers. Because of this observation, successive slabs must rotate about $360^\circ/32$ and are arranged in 32-fold helical noncrystallographic symmetry (Figure 5), and the amyloid fibers and their sheets are then twisted. Without this twisting, the repeat unit along this axis would be reduced to $c = 4.8 \text{ \AA}$. This is the direct observation corresponding to a specific twisting value, which we include as an important constraint in our model.

Sheets within amyloid fibers have different curvatures in twisted structures, depending on their distance to the fiber axis (Figures 5B and 6). Four sheets in our model can be divided into two inner and two outer sheets (Figure 6B). Both sides of the inner sheets, likely with a high content of hydrophobic residues, are capable of interactions with other β sheets, while only one side of the outer sheets is required to be so. As discussed above, β sheets formed by any set of sequences have an intrinsic curvature and have their own sidedness of hydrophobic residues. Only when the intrinsic curvature of predicted sheets matches the geometric requirement of two inner and two outer sheets (Figure 6) does the B1 domain form amyloid fibers. This may be a general requirement for other amyloid fiber-forming proteins based on cross- β structure.

Backbone hydrogen bonds within the outer sheets force their strands to tilt against the equatorial axis by about 35° (Figure 6C). When slabs twist in stacking, the strand-strand distances between the two adjacent slabs increase at the ends of strands (Figure 5B), while they remain constant at the middle. Because of backbone hydrogen bonds, the strand-strand distances must remain approximately constant at about 4.8 \AA throughout the strands. A tilting of strands within each slab is necessary. For a given twist of slabs, the distance effects on the outer sheets are much larger than on the inner sheets. In general, tilting of strands in the outer sheets is sufficient. On the basis of modeling, the tilting is approximately 35° . With this tilting, the strand-strand distances in the outer sheets are slightly longer than those in the inner sheets. Such tilting would cause the meridional 4.8 \AA reflection to extend as an arc from the meridional axis by about the same amount. Indeed, one sees such an arc even in the nearly perfectly aligned samples of A β 11–25 (Serpell, 2000; Sikorski et al., 2003).

Helical twisting of amyloid fibers has been seen in the electron microscopy for both disease and non-disease-associated proteins (Blake and Serpell, 1996; Sunde et al., 1997). The X-ray data we present provide additional evidence for, and quantification of, fiber superhelical twisting.

All cross- β amyloid fibers seem to have a common core structure, regardless of the sequence of proteins involved (Sunde et al., 1997). The previous model for the core of transthyretin amyloid fibrils has a diameter of about 50 \AA and a fiber repeat of 116 \AA , corresponding to 24 slabs. Our fibers fit the unit cell of $40 \text{ \AA} \times 40 \text{ \AA} \times 154 \text{ \AA}$, corresponding to 32 slabs. Our fiber should have a diameter of 45 \AA in solution after conversion from the square slab to a cylinder model. Blake et al.'s model (Sunde et al., 1997) simply twists more and is thicker than ours, while the volumes of the two models are within 8% of each other. Below, we provide the structural and geometric basis for why the two amyloid fi-

bers have the same volume as the fiber unit, the same number of sheets (four), and a similar strand length.

Geometry of Twisted β Sheets: Length of β Strands and Number of Sheets

There is no limit on the length of strands and the number of stacked sheets when sheets are flat and do not undergo twisting. However, sheets of naturally occurring parallel β strands have intrinsic twisting around the direction of β strands (Richardson, 1981). This is due to the maximization of side chain interactions. Here, we proposed a tilting of strands around two other directions for maintaining backbone interactions. Because of backbone hydrogen bonds in the successively stacked slabs that twist around the fiber axis, strands in the outer sheets further tilt around the equatorial axis by 35° , as described above. This tilting makes the spiral passage of outer sheets longer than that of inner sheets, which wrap tangentially around cylinders. The passage length of the outer sheets and the tilting angles of their strands set the geometric limits on the number of sheets and the length of strands in the twisted structure, respectively.

The strand length is about 5 residues in our structure. Clearly, 3 residues is a minimal number to be considered to be a part of a sheet. Maximal length, which is set by the width of the slab, will not exceed 11 residues (Figure 5). Due to 11.25° twisting of slabs, the lateral displacement at the amino- and carboxyl-terminal ends of 5-residue strands of the outer sheets is about 3.5 \AA . Computer modeling and energy minimization shows that a strand tilt of about 35° around an equatorial axis could continue to maintain backbone hydrogen bonds at both ends between two adjacent slabs. A similar geometry of backbone hydrogen bonds would be much more difficult to maintain at the ends of strands longer than 5 residues, because further tilting of strands, with a substantial increase of the passage length of the sheets, may not occur.

The maximal number of sheets in our structure is four. This has been set by the X-ray diffraction data. Additionally, it is also set by geometry. When an additional sheet is added onto either side of our structure, the sheet cannot maintain backbone hydrogen bonds, because a strand tilting of more than 35° or a further increase of the passage length of the sheet is not possible. This limit on the number of sheets may be applicable to all twisted cross- β amyloid fibers.

Although detailed atomic structure of the amyloid fiber-forming slab and thus the amyloid fiber is beyond the scope of this study, the slab should contain about half the number of residues in the core β strand structure for the formation of four sheets (Figure 5), and the remaining half of the residues are in the unstructured connecting loops (not shown).

Our Model in the Context of Other Structural Studies on Fibers

Here, we provide a structural model for the twisted cross- β structure of an amyloid fiber on the basis of X-ray diffraction data. The existence of multiple sheets appears to be a common feature among all cross- β structures of amyloid fibers with characteristic reflec-

tions at 4.7–4.8 Å and 10–11 Å (Sunde et al., 1997; Malinchik et al., 1998; Serpell, 2000; Serpell et al., 2000; Dobson, 2003). A single-sheeted β helix model was recently proposed to be a general model for the amyloid fibers (Govaerts et al., 2004). However, this model has only one sheet and should not give rise to an observable reflection for the sheet-sheet stacking, which was reported to be at 8.82 Å resolution (Nguyen et al., 1995). This model is not applicable to any amyloid fibers that have multiple sheets, as shown in diffraction data typically at about 10–11 Å resolution (Sunde et al., 1997; Serpell, 2000).

Eisenberg and colleagues have proposed another cross- β structure, but one without any helical twisting (Balbirnie et al., 2001; Diaz-Avalos et al., 2003). Their model was based on high-resolution diffraction studies for fibers formed by a 7 amino acid peptide (GNNQ QNY) derived from the yeast prion protein Sup35. This peptide lacks any hydrophobic residues, and its amyloid model is not subject to the connectivity constraint. If we had not collected all X-ray diffraction data, especially the two lowest-resolution reflections near the beam stop, we would have also been led to adopt an amyloid model without any twisting. We used a very small beam stop that was required to avoid obliterating this part of the diffraction pattern.

Experimental Procedures

Amyloid Fiber Preparation and Alignment

The “AY” mutant of the IgG binding B1 domain of streptococcal protein G (Figure 1A), or B1(AY), was used in this study and has been extensively described and characterized previously (Merkel and Regan, 1998; Ramirez-Alvarado et al., 2000, 2003; Ramirez-Alvarado and Regan, 2002). Briefly, the protein samples were prepared and stored in 50 mM sodium acetate (pH 5.2). Amyloid fibers were formed during agitation and incubation near the melting temperature ($T_m = 334$ K) for about 36 hr. Fibers were pelleted by centrifugation, and the supernatant was discarded. The fibers were extensively washed with distilled water, recentrifuged, and resuspended in either distilled water or 50 mM or 100 mM NaCl. The fibers were pipetted into solvent-filled 0.7 mm quartz capillaries. The capillaries were centrifuged for 24 hr, 72 hr, 1 week, or longer in a swinging bucket rotor at 4°C at 2000 \times g. Excess buffer was removed, and the samples were then let to dry at room temperature. Alternatively, a drop of fiber solution was placed between two capillary ends and allowed to dry (stretching frame).

Six capillary samples were allowed to dry slowly, by evaporation over a 6 month period. All samples showed a typical diffraction pattern of fibers, but one sample showed a powder diffraction pattern to atomic resolution. This sample was originally prepared by resuspension in 50 mM NaCl (which also resulted in some powders of NaCl crystals). This sample had reflections to the edge of the detector.

Electron Microscopic Imaging

Samples were prepared by applying a drop of fiber solution to a formvar-coated copper grid. The grids were stained with 1% (w/v) phosphotungstic acid (PTA) solution (pH 7) and air dried. The samples were examined with a Zeiss JEM transmission electron microscope at 80 kV excitation voltage.

X-Ray Diffraction, Radial Integration, and Indexing

Routine X-ray diffraction experiments were carried out for the prepared samples before and after centrifugation and drying, using both Raxis-IV and Mar imaging systems with a home radiation source operated at 50 kV and 100 mA at the Center for Structural Biology at Yale University. Still diffraction images were taken with typical exposure times of 20, 60, 90, and 120 min with the sample-to-detector distances of 110, 125, and 150 mm. In order to observe

very low-resolution reflections, we designed a very small beam stop and placed it as far away as possible from the sample (90 mm). The alignment of the beam stop was carried out by using fluorescent inorganic salt crystals molded in small balls as well as by using the powder form of NaCl crystals. When the beam stop was placed at 90 mm, the closest sample-to-detector distance was about 110 mm, which limited the highest resolution detected at the edge of the detector to 1.6 Å resolution. Additional X-ray diffraction for one sample was carried out at Argonne National Laboratory.

Radial integration of the diffraction pattern was carried out with the program FIT2D (Hammersley, 1998), after the detector geometry and radiation source properties were calibrated by using the (200) reflection of the standard NaCl powder diffraction. NaCl crystals belong to the isomeric hexoctahedral space group Fm-3m (space group number = 225) with the cell dimensions of $a = b = c = 5.6402$ Å. At the detector distance of 110 mm, there were three NaCl reflections observed: (200) at the resolution of 2.821 Å, (220) at 1.994 Å, and (222) at 1.628 Å. Individual reflections of residual NaCl crystals were masked out before radial integration of diffraction pattern.

Indexing was carried out in a brute-force search routine upon matching the resolutions of the observed 17 strong reflections to calculated ones. The search was performed in two dimensions, because the third dimension (c axis) along the fiber axis has a very long dimension, $c = 153.6$ Å, and diffracts weakly to only a few orders of reflections. The search under the condition of $a = b = 10$ to 45 Å with the increment of 0.01 Å and fixed $\alpha = \beta = \gamma = 90^\circ$ resulted in one solution with the acceptable discrepancy of 0.02 Å in resolution between each calculated and observed reflection. This solution ($a = b = 39.83$ Å) also matched resolutions of an additional 12 weak reflections. Another solution was found: $a = 20.60$ Å, $b = 21.34$ Å, $\gamma = 103.5^\circ$, in the search under the condition that a, b (from 3 to 30 Å), and γ (from 90 to 135°) varied independent with the increment 0.01 Å and 0.5°, respectively. We discarded the second solution, because it could only accommodate one-third of one subunit per layer.

Fourier Transformation of Amyloid Models and Graphics

Fourier transformation of our two models as described in Figure 6 was carried out without radial averaging by using the program FFT of CCP4 (CCP4, 1994) in order to validate the basic features of diffraction patterns. In both models (uniform $B = 20$ Å²), we observed a large blind diffraction cone (Cochran et al., 1952; Wilkins et al., 1953; Taylor and Lipson, 1965) of about 60°. This cone starts with $l = 0$ and intersects with another inverted blind cone starting with $l = 32$. This is precisely the expected cone angle, $\alpha = \cos^{-1}(2D/c)$, where a helical repeat unit $c = 153.6$ Å and a diameter of helix $D = 2(A/\pi)^{1/2} = 45$ Å, where A is the area of the slab. In this calculation, perfect 32-fold helical NCS was used, and all reflections within the blind cone, including reflections (001) and (002), had zero intensity. Considering possible imperfect NCS, these reflections would have small but non-zero measurable intensities.

Graphics programs Ribbons (Carson, 1991) and Midas (Ferrin et al., 1988) were used for making Figures 1A, 5, and 6.

Acknowledgments

L.R. gratefully acknowledges the support of the National Institutes of Health (GM57265). J.W. acknowledges Yale University for the support of the directorship of the Center for Structural Biology. S.G. thanks Barry Piekos, Yale University for access to the TEM and for his advice in its use. We thank Aitziber López Cortajarena, Christopher Wilson, Irina Pozdnyakova, Janani Venkatraman, Thomas Magliery, Tommi Kajander, Simon Mochrie, and Peter Moore for discussions and thoughtful comments on the manuscript.

Received: February 21, 2005

Revised: June 8, 2005

Accepted: June 14, 2005

Published: September 13, 2005

References

Åkerström, B., Brodin, T., Reis, K., and Björck, L. (1985). Protein G: a powerful tool for binding and detection of monoclonal and polyclonal antibodies. *J. Immunol.* 135, 2589–2592.

- Alexander, P., Fahnestock, S., Lee, T., Orban, J., and Bryan, P. (1992a). Thermodynamic analysis of the folding of the streptococcal protein G IgG-binding domains B1 and B2: why small proteins tend to have high denaturation temperatures. *Biochemistry* *31*, 3597–3603.
- Alexander, P., Orban, J., and Bryan, P. (1992b). Kinetic analysis of folding and unfolding of the 56 amino acid IgG-binding domain of streptococcal protein G. *Biochemistry* *31*, 7243–7248.
- Balbirnie, M., Grothe, R., and Eisenberg, D.S. (2001). An amyloid-forming peptide from the yeast prion Sup35 reveals a dehydrated β -sheet structure for amyloid. *Proc. Natl. Acad. Sci. USA* *98*, 2375–2380.
- Björck, L., and Kronvall, G. (1984). Purification and some properties of streptococcal protein G, a novel IgG-binding reagent. *J. Immunol.* *133*, 969–974.
- Blake, C., and Serpell, L. (1996). Synchrotron X-ray studies suggest that the core of the transthyretin amyloid fibril is a continuous β -sheet helix. *Structure* *4*, 989–998.
- Bucciantini, M., Giannoni, E., Chiti, F., Baroni, F., Formigli, L., Zurdo, J., Taddei, N., Ramponi, G., Dobson, C.M., and Stefani, M. (2002). Inherent toxicity of aggregates implies a common mechanism for protein misfolding diseases. *Nature* *416*, 507–511.
- Carson, M. (1991). Ribbons 2.0. *J. Appl. Crystallogr.* *24*, 958–961.
- CCP4 (Collaborative Computational Project, Number 4)(1994). The CCP4 suite: programs for protein crystallography. *Acta Crystallogr. D Biol. Crystallogr.* *50*, 760–763.
- Chiti, F., Webster, P., Taddei, N., Clark, A., Stefani, M., Ramponi, G., and Dobson, C.M. (1999). Designing conditions for in vitro formation of amyloid protofilaments and fibrils. *Proc. Natl. Acad. Sci. USA* *96*, 3590–3594.
- Cochran, W., Crick, F.H.C., and Vand, V. (1952). The structure of synthetic polypeptides. I. The transformation of atoms on a helix. *Acta Crystallogr.* *5*, 581.
- Der-Sarkissian, A., Jao, C.C., Chen, J., and Langen, R. (2003). Structural organization of alpha-synuclein fibrils studied by site-directed spin labeling. *J. Biol. Chem.* *278*, 37530–37533.
- Diaz-Avalos, R., Long, C., Fontano, E., Balbirnie, M., Grothe, R., Eisenberg, D., and Caspar, D.L.D. (2003). Cross-beta order and diversity in nanocrystals of an amyloid-forming peptide. *J. Mol. Biol.* *330*, 1165–1175.
- Dobson, C.M. (2003). Protein folding and misfolding. *Nature* *426*, 884–890.
- Ferrin, T.E., Huang, C.C., Jarvis, L.E., and Langridge, R. (1988). The MIDAS display system. *J. Mol. Graph.* *6*, 13–27.
- Gallagher, T., Alexander, P., Bryan, P., and Gilliland, G.L. (1994). Two crystal structures of the B1 immunoglobulin-binding domain of streptococcal protein G and comparison with NMR. *Biochemistry* *33*, 4721–4729.
- Gordon, D.J., Balbach, J.J., Tycko, R., and Meredith, S.C. (2004). Increasing the amphiphilicity of an amyloidogenic peptide changes the β -sheet structure in the fibrils from antiparallel to parallel. *Biophys. J.* *86*, 428–434.
- Govaerts, C., Wille, H., Prusiner, S.B., and Cohen, F. (2004). Evidence for assembly of prions with left-handed β -helices into trimers. *Proc. Natl. Acad. Sci. USA* *101*, 8342–8347.
- Gronenborn, A.M., Filipula, D.R., Essig, N.Z., Achari, A., Whitlow, M., Wingfield, P.T., and Clore, G.M. (1991). A novel, highly stable fold of the immunoglobulin binding domain of streptococcal protein G. *Science* *253*, 657–661.
- Gross, M., Wilkins, D.K., Pitkeathly, M.C., Chung, E.W., Higham, C.W., Clark, A., and Dobson, C.M. (1999). Formation of amyloid fibrils by peptides derived from the bacterial cold shock protein CspB. *Protein Sci.* *8*, 1350–1357.
- Guijarro, J.I., Sunde, M., Jones, J.A., Campbell, I.D., and Dobson, C.M. (1998). Amyloid fibril formation by an SH3 domain. *Proc. Natl. Acad. Sci. USA* *95*, 4224–4228.
- Hammersley, A.P. (1998). The European Synchrotron Radiation Facility (ESRF) Internal Report. ESRF98HA01T, FIT2D V9.129 Reference Manual V3.1 (Grenoble, France: ESRF).
- Jimenez, J.L., Guijarro, J.I., Orlova, E., Zurdo, J., Dobson, C.M., Sunde, M., and Saibil, H.R. (1999). Cryo-electron microscopy structure of an SH3 amyloid fibril and model of the molecular packing. *EMBO J.* *18*, 815–821.
- Jimenez, J.L., Nettleton, E.J., Bouchard, M., Robinson, C.V., Dobson, C.M., and Saibil, H.R. (2002). The protofilament structure of insulin amyloid fibrils. *Proc. Natl. Acad. Sci. USA* *99*, 9196–9201.
- Koide, S., Huang, X., Link, K., Koide, A., Bu, Z., and Engelman, D.M. (2000). Design of single-layer β -sheets without a hydrophobic core. *Nature* *403*, 456–460.
- Kuszewski, J., Gronenborn, A.M., and Clore, G.M. (1999). Improving the packing and accuracy of NMR structures with a pseudopotential for the radius of gyration. *J. Am. Chem. Soc.* *121*, 2337–2338.
- Malinchik, S., Inouye, H., Szumowski, K., and Kirschner, D. (1998). Structural analysis of Alzheimer's beta(1–40) amyloid: protofilament assembly of tubular fibrils. *Biophys. J.* *74*, 537–545.
- Makin, O.S., Atkins, E., Sikorski, P., Johansson, J., and Serpell, L.C. (2005). Molecular basis for amyloid fibril formation and stability. *Proc. Natl. Acad. Sci. USA* *102*, 315–320.
- Martin, R.W., and Zilm, K.W. (2003). Preparation of protein nanocrystals and their characterization by solid state NMR. *J. Magn. Reson.* *165*, 162–174.
- Merkel, J.S., and Regan, L. (1998). Aromatic rescue of glycine in β -sheets. *Fold. Des.* *3*, 449–455.
- Merkel, J.S., Sturtevant, J.M., and Regan, L. (1999). Side-chain interactions in parallel β -sheets: The energetics of cross-strand pairings. *Struct. Fold. Des.* *7*, 1333–1343.
- Naiki, H., Higuchi, K., Hosokawa, M., and Takeda, T. (1989). Fluorometric determination of amyloid fibrils *in vitro* using the fluorescent dye, thioflavin T1. *Anal. Biochem.* *177*, 244–249.
- Nguyen, J.T., Inouye, H., Baldwin, M.A., Fletterick, R.J., Cohen, F.E., Prusiner, S.B., and Kirschner, D.A. (1995). X-ray diffraction of scapic prion rods and PrP peptides. *J. Mol. Biol.* *252*, 412–422.
- Oda, T., Makino, K., Yamashita, I., Namba, K., and Maeda, Y. (1998). Effect of the length and effective diameter of F-actin on the filament orientation in liquid crystalline sols measured by X-ray fiber diffraction. *Biophys. J.* *75*, 2672–2681.
- Petkova, A.T., Ishii, Y., Balbach, J.J., Antzutkin, O.N., Leapman, R.D., Delaglio, F., and Tycko, R. (2002). A structural model for Alzheimer's β -amyloid fibrils based on experimental constraints from solid state NMR. *Proc. Natl. Acad. Sci. USA* *99*, 16742–16747.
- Petkova, A.T., Buntkowsky, G., Dyda, F., Leapman, R.D., Yan, W.M., and Tycko, R. (2004). Solid state NMR reveals a pH-dependent antiparallel β -sheet registry in fibrils formed by a β -amyloid peptide. *J. Mol. Biol.* *335*, 247–260.
- Puchtler, H., Sweat, F., and Levine, M. (1961). On the binding of Congo red by amyloid. *J. Histochem. Cytochem.* *10*, 355–364.
- Ramirez-Alvarado, M., and Regan, L. (2002). Does the location of a mutation determine the ability to form amyloid fibrils? *J. Mol. Biol.* *323*, 17–22.
- Ramirez-Alvarado, M., Merkel, J.S., and Regan, L. (2000). A systematic exploration of the influence of the protein stability on amyloid fibril formation *in vitro*. *Proc. Natl. Acad. Sci. USA* *97*, 8979–8984.
- Ramirez-Alvarado, M., Cocco, M.J., and Regan, L. (2003). Mutations in the B1 domain of protein G that delay the onset of amyloid fibril formation *in vitro*. *Protein Sci.* *12*, 567–576.
- Richardson, J.S. (1981). The anatomy and taxonomy of protein structure. *Adv. Protein Chem.* *34*, 167–339.
- Serpell, L.C. (2000). Alzheimer's amyloid fibrils: structure and assembly. *Biochim. Biophys. Acta* *1502*, 16–30.
- Serpell, L.C., and Smith, J.M. (2000). Direct visualisation of the β -sheet structure of synthetic Alzheimer's amyloid. *J. Mol. Biol.* *299*, 225–231.
- Serpell, L.C., Blake, C.C.F., and Fraser, P.E. (2000). Molecular structure of a fibrillar Alzheimer's A β fragment. *Biochemistry* *39*, 13269–13275.
- Smith, C.K., and Regan, L. (1995). Guidelines for protein design: the energetics of β sheet side chain interactions. *Science* *270*, 980–982.
- Smith, C.K., Withka, J.M., and Regan, L. (1994). A thermodynamic

scale for the β -sheet forming tendencies of the amino acids. *Biochemistry* **33**, 5510–5517.

Sikorski, P., Atkins, E.D.T., and Serpell, L.C. (2003). Structure and texture of fibrous crystals formed by Alzheimer's A β (11–25) peptide fragment. *Structure* **11**, 915–926.

Sunde, M., Serpell, L.C., Bartlam, M., Fraser, P.E., Pepys, M.B., and Blake, C.C. (1997). Common core structure of amyloid fibrils by synchrotron X-ray diffraction. *J. Mol. Biol.* **273**, 729–739.

Taylor, C.A., and Lipson, H. (1965). *Optical Transformations, Their Preparation and Application to X-Ray Problems* (Ithaca, NY: Cornell University Press).

Wilkins, M.H., Stokes, A.R., and Wilson, H.R. (1953). Molecular structure of deoxyribose nucleic acids. *Nature* **171**, 738–740.

Yamashita, I., Suzuki, H., and Namba, K. (1998). Multiple-step method for making exceptionally well-oriented liquid-crystalline sols of macromolecular assemblies. *J. Mol. Biol.* **278**, 609–615.